JGR Atmospheres

RESEARCH ARTICLE
10.1029/2025JD044310

Synoptic Features Driving the CO_2 Sink in the Mediterranean Sea in Winter

M. Reale[1], F. Giordano[1,2], V. Di Biagio[1], G. Cossarini[1], and S. Salon[1]

[1]National Institute of Oceanography and Applied Geophysics–OGS, Trieste, Italy, [2]University of Trieste, Trieste, Italy

Key Points:

- High CO_2 sink events in the Mediterranean take place in presence of specific large-scale configurations
- These synoptic configurations are responsible for stronger (colder)-than-average wind (temperature) patterns in the region
- The larger the intensity of the CO_2 sink event, the higher the probability of detecting a cyclone nearby

Correspondence to:

M. Reale,
mreale@ogs.it

Citation:

Reale, M., Giordano, F., Di Biagio, V., Cossarini, G., & Salon, S. (2026). Synoptic features driving the CO_2 sink in the Mediterranean Sea in winter. *Journal of Geophysical Research: Atmospheres*, *131*, e2025JD044310. https://doi.org/10.1029/2025JD044310

Received 9 MAY 2025
Accepted 24 DEC 2025

Abstract The Mediterranean Sea is a weak sink for the atmospheric CO_2 with the October-March extended winter season characterized by the occurrence of high CO_2 sink events. Here, we analyzed state-of-the-art ocean and atmospheric reanalyses and observational data sets to investigate the variability of the winter sink and its relation with synoptic atmospheric features crossing the region in the period 1999–2020. High CO_2 sink events are identified using classical extreme event approach with fixed threshold (95p) based on the CO_2 daily flux distribution. First, we showed that these events are driven by large-scale atmospheric configurations that produce stronger-than-average wind speed and colder-than-average 2 m and sea surface temperature patterns in the region. Second, a co-location analysis was applied to assess the probability to detect an extra-tropical cyclone at a fixed distance from the location of the events showing that the larger the event's magnitude, the higher the probability. In most of the cases, these cyclones originate within the Mediterranean region and are usually deeper, bigger in terms of size and characterized by a stronger circulation with respect to the systems that usually cross the region. By establishing a statistical relationship between high CO_2 sink events and synoptic atmospheric activity, we emphasize the potential influence of the cyclone activity on the carbon budget of the Mediterranean Sea.

Plain Language Summary The Mediterranean acts as a weak CO_2 sink along the year. Here, by using state-of-the-art ocean and atmospheric data sets available for the region, the temporal variability of the extreme events of CO_2 absorption and their links with weather and ocean patterns and with the passage of extratropical cyclones in the region have been investigated. The analysis points out that the extreme events of CO_2 absorption take place in presence of large-scale configurations that produce stronger-than-average wind speed and colder-than-average temperature patterns in the region. Moreover, it points out the high probability, with respect to the climatology, to find a cyclone nearby the location of each event. These cyclones associated with high CO_2 sink events mostly originated in the Mediterranean region and are usually stronger and bigger in terms of size with respect to those that usually cross the area. Due to the importance of these CO_2 sink events in the carbon anthropogenic storage of the basin, the projected decrease in the cyclones frequency in the area could significantly affect the sinking character of the basin in the future.

1. Introduction

The Mediterranean region (hereafter MEDIT, Figures 1a and 1b) is a midlatitude continental area encompassing the southern part of Europe, the northern part of Africa, and part of the Middle East that is characterized by several complex and different environmental and societal dynamics (e.g.., Lionello et al., 2012) and by the presence of a semienclosed basin, the Mediterranean Sea (hereafter MS, Figure 1b).

The MS is connected through the Gibraltar Strait with the Atlantic Ocean and through the Dardanelles Strait with the Black Sea and is widely recognized as an "ocean in miniature" where air-sea interactions, wind stress, and exchanges at Gibraltar Strait drive the dynamics and intensity of three different thermohaline cells (e.g., Schroeder et al., 2012). From a biogeochemical point of view, the MS is an oligotrophic basin (ultra-oligotrophic in its eastern part) characterized by low values of net primary production with respect to the global ocean (e.g., Siokou-Frangou et al., 2010; Lazzari et al., 2012; Stambler, 2014; Reale et al., 2022and references therein). Moreover, a peculiar east-west trophic gradient arises from differences in the stratification regimes of the basin (i.e., east basin is almost permanently stratified), negative nutrient inflow/export imbalance at Gibraltar, anti-estuarine basin-wide circulation, and uneven distribution of rivers and convective areas (Álvarez et al., 2023; Crise et al., 1999; Crispi et al., 2001; Lazzari et al., 2012, 2016). Observational and modeling studies have identified the MS as a weak sink for the atmospheric CO_2 (Alvarez et al., 2014; Canu et al., 2015; Carranceno

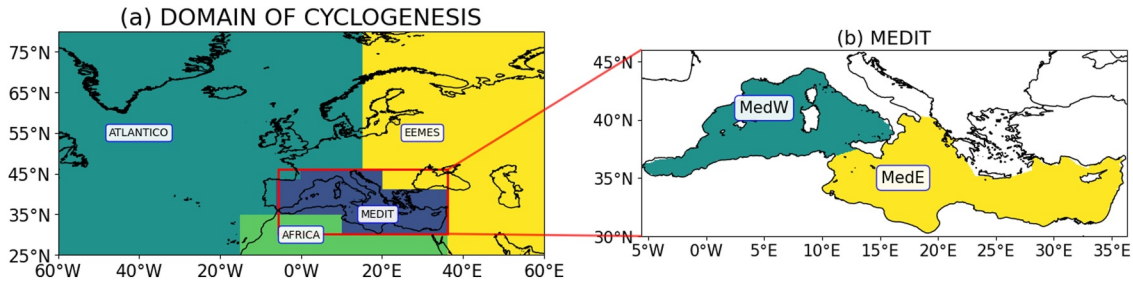

Figure 1. (a) The Mediterranean region (MEDIT) together with the other areas identified for the cyclogenesis processes: Atlantic Ocean (ATLANTICO), northern Africa (AFRICA), and eastern Europe/Middle East (EEMES); (b) division of the Mediterranean Sea in two sub-basins, that is, western (MedW) and eastern (MedE) Mediterranean Sea.

et al., 2018; Cossarini et al., 2021; D'Ortenzio et al., 2008). Although the MS is a warm, high-alkalinity basin with a high Revelle factor, it generally acts as a net sink for atmospheric CO_2 (approximately 17.8 million ton year^{-1}, Canu et al., 2015) that is removed from the surface through the overturning circulation and then exported through the Gibraltar strait contributing to the anthropogenic carbon storage in the North-East Atlantic (Alvarez et al., 2014; Cossarini et al., 2015; Carraceno et al., 2018; Cossarini et al., 2021; Frangoulis et al., 2024 and reference therein). The largest CO_2 absorption takes place in the western Mediterranean in winter, mirroring the aforementioned east-west trophic gradient, the latitudinal distribution of the sea temperature, and the seasonality of the biological activity (Canu et al., 2015; Cossarini et al., 2021; Frangoulis et al., 2024).

CO_2 flux across the air-sea interface ($\mathbf{FCO_2}$) is estimated (e.g., Gutiérrez-Loza et al., 2022) as follows:

$$\mathbf{FCO_2 = kK_o\left(pCO_2^w - pCO_2^a\right)} \quad (1)$$

with $\mathbf{pCO_2^w}$ and $\mathbf{pCO_2^a}$ partial pressure of CO_2 in the ocean and atmosphere respectively, $\boldsymbol{k}$ gas transfer velocity, and $\boldsymbol{K_0}$ solubility constant dependent on salinity and temperature of the water (Weiss, 1974). Although $\boldsymbol{K_0}$ solubility mostly depends on temperature, $\boldsymbol{k}$ depends on wind with a quadratic form (e.g., Wanninkhof, 2014). Thus, high wind speed can play an important role in shaping the spatiotemporal variability of $\mathbf{FCO_2}$.

From this point of view, MEDIT is characterized by the presence of several strong winds, namely Mistral, Tramontana, Sirocco, Etesian, Bora, Khamsin, or Sharav (e.g., Lionello et al., 2006; Ulbrich et al., 2012), which are characterized by definite location, behaviors, and characteristics and because of that they are generally recognized as "local winds." Features and the intensity of these winds have been often connected to the extra-tropical cyclones crossing the region (e.g., Lionello et al., 2006; Nissen et al., 2010, 2014; Ulbrich et al., 2012). For example, in the case of Mistral, the weather systems which cause these winds are located within the Mediterranean, in or very near the Gulf of Genoa, often generated by lee cyclogenesis (e.g., Buzzi et al., 2020). For the sirocco wind, the same systems are usually located over or westwards with respect to Italy (Lionello et al., 2006).

The role of the extra-tropical cyclones in influencing the hydrological cycle and the location and intensity of several meteorological extremes in the region has been widely acknowledged (e.g.,: Flaounas et al., 2022; Lionello et al., 2006; Lionello et al., 2019; Nissen et al., 2010, 2014; Portal et al., 2024; Reale et Lionello, 2013; Reale et al., 2021; Ulbrich et al., 2012). However, the same is not true in the case of the extremes in the marine environment. In fact, only a few studies have recently shed light on the effects of the passage of different weather systems on the marine environment in the MS. For example, Menna et al. (2023) described, for the first time, the interaction between an extreme weather system (i.e., Medicane Apollo) and an ocean cyclonic gyre located in the western Ionian Sea at the end of October 2021. As a consequence of the passage of the system, in situ floats and surface drifters observed a significant drop in the temperature at the core of the gyre due to a local maximum in the wind-stress curl associated with the weather system and a significant increase in oxygen solubility, chlorophyll-a, and productivity at the surface. On the other hand, Jangir et al. (2024) examined the case of three different medicanes (i.e., Zorbas, Ianos, and Apollo) and analyzed their interactions with different warm core eddies encountered along their tracks. In the case of Zorbas and Apollo, they observed an increase in the chlorophyll-a and phytoplankton concentration after the passage of the systems. Marked changes in surface ocean fields such as

an increase of currents intensity, sea level, significant wave height, chlorophyll-a, and a decrease of temperature during the Medicane Ianos (17–20 September 2020) were detected by the Copernicus Marine Service and described by Clementi et al. (2022).

Several observational studies carried out in the tropics and subtropics have revealed a strong local influence of extra-tropical and tropical weather systems on the air-sea CO_2 exchanges (e.g., Carranza et al., 2024 and references therein) as a consequence of the wind forcing and drop of the surface temperature associated with the passage of the systems. On the other hand, in the MEDIT, to the best of our knowledge, no studies have carried out an analysis of the response of the CO_2 air-sea fluxes and related extremes to the interaction with atmospheric systems.

In this work, we aim at: (a) characterizing the spatiotemporal variability during the extended winter season October-March of the period 1999–2020 of high CO_2 sinks events in the MS (see next section for details) identified through a classical extreme detection approach, (b) investigating the links between these events, large-scale circulation patterns, atmospheric and ocean variables, and extra-tropical cyclones crossing the region, (c) assessing the sensitivity of this link to the choice of the threshold of the intensity of the event, and (d) describing the characteristics of cyclones associated with these events when the threshold of the intensity of the event is changed. Section 2 describes the data and methodology used in the study. In particular, the analysis is based on the use of state-of-the-art data sets for both ocean and atmosphere available for the region: the Mediterranean Sea Biogeochemistry reanalysis (Cossarini et al., 2021), the daily high resolution L4 Sea Surface Temperature (SST) reprocessed long-term SST of the Copernicus Marine Service (Embury et al., 2024; Pisano et al., 2016), and the ECMWF atmospheric reanalysis ERA5 (Hersbach et al., 2020, 2023). The data set of cyclone tracks has been produced by applying a cyclone detection and tracking algorithm (Lionello et al., 2002; Reale & Lionello, 2013) to the 6-hourly 0.25° Mean Sea Level Pressure (MSLP) ERA5 fields. Section 3 describes the characteristics of the high CO_2 sink events of the atmospheric and ocean patterns and of the cyclones associated with these events. Section 4 provides a brief summary and the main conclusions of the work.

2. Data and Methods

Daily 2D CO_2 air-sea fluxes for the period 1999–2020 at 1/24° horizontal resolution were retrieved from the marine biogeochemistry reanalysis data set available within the Copernicus Marine Service (hereafter CMS, Cossarini et al., 2021). The data set has been built using the MedBFM modeling system (Salon et al., 2019), which is based on the coupling between the OGSTM transport model (hereafter OGSTM, Lazzari et al., 2012, 2016), the biogeochemical flux model BFM (Vichi et al., 2020), and the 3DVarBio variational scheme that assimilates weekly satellite surface chlorophyll-a concentrations (Teruzzi et al., 2019). MedBFM is forced by the CMS Mediterranean Sea physical reanalysis (Escudier et al., 2021) and by ECMWF atmospheric reanalysis ERA5 (Hersbach et al., 2020) that, respectively, provide at a daily frequency zonal and meridional component of the ocean currents, temperature, salinity, diffusivity, solar radiation, and wind.

The carbonate system variables along with the full set of physical and biogeochemical reanalysis products were extensively validated across multiple spatial and temporal scales (see Cossarini et al., 2021; Escudier et al., 2021; Teruzzi, Di Biagio, et al., 2021, Teruzzi, Feudale, et al., 2021). Although high-frequency observational time series were not available, this comprehensive validation supports the reliability of the model in representing air-sea CO_2 flux dynamics at daily and 1/24° horizontal resolution.

Following previous analysis (Canu et al., 2015; Reale, Giorgi, et al., 2020, Reale, Salon, et al., 2020), the MS has been divided into two sub-basins: MedW (Western) and MedE (Eastern) Mediterranean (Figure 1b). The Adriatic Sea and the Aegean Sea were excluded since their biogeochemical dynamics has been shown to be often significantly influenced by river discharge, which can fuel or dump the trophic web activity in both basins masking or mimicking (even in the open ocean areas) the action of the large-scale circulation patterns (e.g., Reale, Salon, et al., 2020). It is important to remind that the analysis has been focused only positive CO_2 air-sea fluxes (that correspond to fluxes from the atmosphere into the ocean and thus absorption) during the extended winter period October-March, when the MS acts as sink for the atmospheric CO_2 and the cyclone activity in MEDIT is at its highest level (Flaounas et al., 2022; Lionello et al., 2006, 2016; Ulbrich et al., 2012).

High CO_2 sinks events (hereafter EEs) were then identified using the extreme event detection tool described by Di Biagio (2017) and applied to chlorophyll-a (Di Biagio et al., 2020) and current speed data (Giordano et al., 2024).

Briefly, the method first detects the domain cells where a specific threshold q (in this case the 95th percentile separately computed for each sub-basin, hereafter 95p; other thresholds −70th, 80th, and 90th percentiles-were also used throughout the analysis and referred to accordingly) is overcome. Then it finds connected regions, in time and space, of these cells to identify the EEs. Each EE is characterized in terms of temporal and spatial extension (i.e., duration D, from the start to the end date of the EE, and area A, averaged over its duration), persistence (i.e., uniformity U, defined as the ratio of the longitude × latitude × time dimensional volumes of the EEs and of their bounding boxes), and intensity (excess E, defined as the value over the threshold). The implementation of the tool to the daily time series of 2D winter maps of CO_2 exchanges provides a list of EEs and, for each EE that is considered independent from the others taking in place in the basin (eventually at the same time), its dates of start and end, the location (in coordinates of longitude and latitude) and the date of appearance of the centroid (defined as the barycenter of the longitude × latitude × time dimensional EE volume), the average area (in km^2) covered by the EE, the CO_2 flux at centroid, the maximum CO_2 flux measured, and the CO_2 average flux (all in mmol m^{-2} day^{-1}) measured during each EE.

To analyze the EEs-related ocean and atmospheric patterns, we used 0.05° daily high resolution L4 SST reprocessed fields from Copernicus Marine Service and 0.25° 6-hourly ERA5 reanalysis MSLP (or MSLP), zonal and meridional component of wind speed, and 2 m temperature fields.

Areas of origin and the tracks of cyclones crossing MEDIT have been identified using an objective procedure applied to ERA5 6-hourly 0.25° MSLP and extensively described by Lionello et al. (2002) and Reale and Lionello (2013) to which the reader is referred. Briefly, the procedure is based on: (a) the search of the minima in the ERA5 MSLP field at a certain time t_o, (b) the partition of the field itself in a certain number of systems by identifying sets of steepest paths leading to the same MSLP minimum, and (c) the reconstruction of the track by joining the location of the same cyclone center in a sequence of n maps at the time $t_1,\ldots,t_n$. The final result of this methodology is a list of cyclone tracks with their position (as a function of time) in coordinates of longitude and latitude and the temporal evolution of some variables characterizing the intensity and size of the system, such as MSLP minimum and Depth, Size and so on (see Reale & Lionello, 2013 for more details). Following Reale et al. (2021), in order to identify the area of origin of the cyclones associated with each class of EEs, we consider four areas (Figure 1a): Atlantic Ocean (ATLANTICO), northern Africa (AFRICA), Mediterranean region (MEDIT) and eastern Europe/Middle East (EEMES).

To qualitatively evaluate the relationship between cyclone passages in the MEDIT and EEs, we adopted the methodology detailed by Reale and Lionello (2013) and Lionello et al. (2019), where it was used to link cyclones with precipitation extremes and storm surges. The procedure consists in the search of a cyclone within a radius of 15° (i.e., approximately 1,600 km) from the location of the centroid of each EE at 12 UTC on the day of the centroid. The choice of the radius of search is a sort of compromise between the different sizes of the systems that affect the dynamics of extremes in the Mediterranean region, namely Atlantic and Mediterranean cyclones. In fact, many intense cyclones crossing northern Europe have a very large radius and actually are able to produce extreme events (storm surges, precipitation, and windstorm) e.g., in the northern Mediterranean even though their center is located at a large distance (e.g., Doensen et al., 2025; Lionello et al., 2019; Nissen et al., 2010; Raveh-Rubin & Wernli, 2015; Reale & Lionello, 2013). If, during this procedure, only one cyclone system is found, it is associated with the EE. If more than one system is found inside the search radius, the closest cyclone is assigned to the EE. The EE remains unassociated with any system when no cyclone is identified. Figure 2 exemplifies the procedure for an EE in February 2006 in the south Tyrrhenian Sea, which was then positively associated with a cyclone. Panel (a) shows an EE taking place on 7 February 2006 whose spatial limits are represented by a red line and the location of its centroid is represented by a red dot. Panel (b) shows the 10 m wind field (arrows), the MSLP field (contour lines), and 2 m temperature (shaded colors) in the same day. The blue line is the track of a cyclone whose center (blue point) is located less than 1600 km at 12 UTC from the centroid of the EE (red point, 7 February 2006).

3. Results

3.1. Spatiotemporal Variability of EEs and Related Synoptic Patterns

The extreme event detection tool applied to daily 2D CO_2 time series found 1733 EEs in MedW and 2180 EEs in MedE. The observed differences reflect not only the different spatial extension of two basins but also the automatic selection of EEs with specific spatial scales. In fact, our tool filters events covering areas smaller than

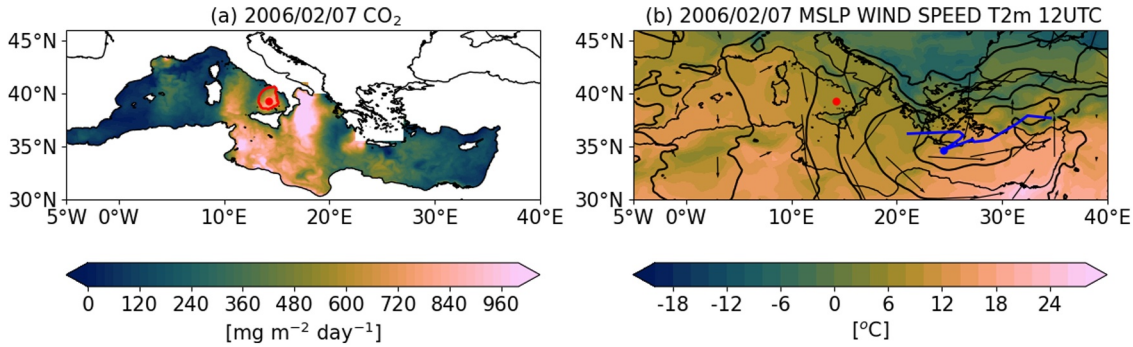

Figure 2. (a) CO_2 air-sea fluxes on 7 February 2006 in mg m^{-2} day^{-1}. Red dot represents the location of the centroid of the EE. Red contour indicates the spatial limit of the EE. (b) Wind fields (arrows, in m/s) and mean sea level pressure (contour lines, in hPa) at 12 UTC on 7 February 2006. Shaded colors are the 2 m temperature in °C. The blue line is the track of the cyclone whose center (blue point) is located less than 1600 km at 12 UTC 7 February 2006 from the centroid of the EE (red point).

900 km^2, that is one order of magnitude lower than that observed in the case of the medicanes (that are the most extreme Mediterranean cyclones and can have a radius of 300 km or more, De La Vara et al., 2021; Emanuel et al., 2025). This choice is based on the need to have comparable spatial scales between EEs and cyclones and filter out small events that can be driven by local dynamics that are not the focus of our study, which is devoted to detect the synoptic forcing of EEs. Figure 3 shows their time series (a, b panels), the seasonal cycle (c, d), and their relative frequency in function of the duration (in number of days, e, f) and average area (in km^2, g, h) for both MedW (a, c, e, g) and MedE (b, d, f, h).

The application of the Mann-Kendall test (Kendall, 1975; Mann, 1945) found the absence of significant trends for the relative frequency of EEs. Moreover, EEs tend to occur at the end of the winter season. For example, more than 60% of EEs take place between December and February, that is the coldest period of the year in the region (Lionello et al., 2012) and the one characterized by higher wind intensity (e.g., Martinez & Iglesias, 2023). In both MedW and MedE, the most likely value of the duration of each EE is one day and almost 90% of EEs have a length lower than 3 days. Moreover, more than 50% of EEs cover an average area smaller than 2*10^5 km^2.

From this point of view, to make also the temporal scale of EEs comparable with those of cyclones crossing the MEDIT (that have, on average, a temporal scale of 22–28 hr; e.g. Trigo et al., 1999; Campins et al., 2011), all the forthcoming analysis has been restricted to all the EEs with a duration smaller or equal to 3 days. This exclusion counted for less than 15% of the total number of the EEs still allowing a robust statistical analysis. In fact, a preliminary comparison of the density of tracks of cyclones associated with all the EEs and with the subset obtained after filtering out all the EEs with duration greater than 3 days (see Figure 8) did not show any significant changes in the spatial patterns and their intensity (not shown here).

Figure 4 shows the composite of MSLP (contours) at 12 UTC on the day of the centroid for EEs in MedW (a) and MedE (b) with shaded colors indicating the anomalies of the MSLP composite with respect to the 1999–2020 ONDJFM climatology. More specifically, each composite has been built by averaging the synoptic fields of MSLP at 12 UTC on the day of the centroid. The red dots represent the average location of the centroid for EEs in MedW and MedE, respectively. The shaded colors are the anomalies of the composites with respect to the ONDJFM climatology for the period 1999–2020. In MedW (a), the composite of MSLP shows clearly the presence of a well-defined minimum located over Italy. Moreover, a strong high-pressure field is located in the Atlantic, somehow elongated toward the western Mediterranean. The spatial gradient resulting from these two rather opposite large-scale circulation patterns has the potential to produce intense and cold winds, which flow mainly from North-West to South-East (e.g., Ragone et al., 2019). A similar configuration is observed in the MedE (b) where, together with the high-pressure that shifted eastwards with respect to that one observed in MedW, there is a minimum located between the Ionian and Cyprus. All the minima are usually deeper than the climatological field: approximately more than 6 and 3 hPa in MedW and in MedE, respectively.

The wind and temperature patterns associated with these large-scale circulation structures are shown in Figures 5 and 6. Both figures show the composite of the 10 m wind fields (Figure 5) and 2 m temperature (Figure 6) at 12 UTC on the day of the centroid in MedW (a) and MedE (b). Again, the shaded colors are the anomalies of the composites with respect to the ONDJFM climatology for the period 1999–2020. Figures 5 and 6 point out that, in

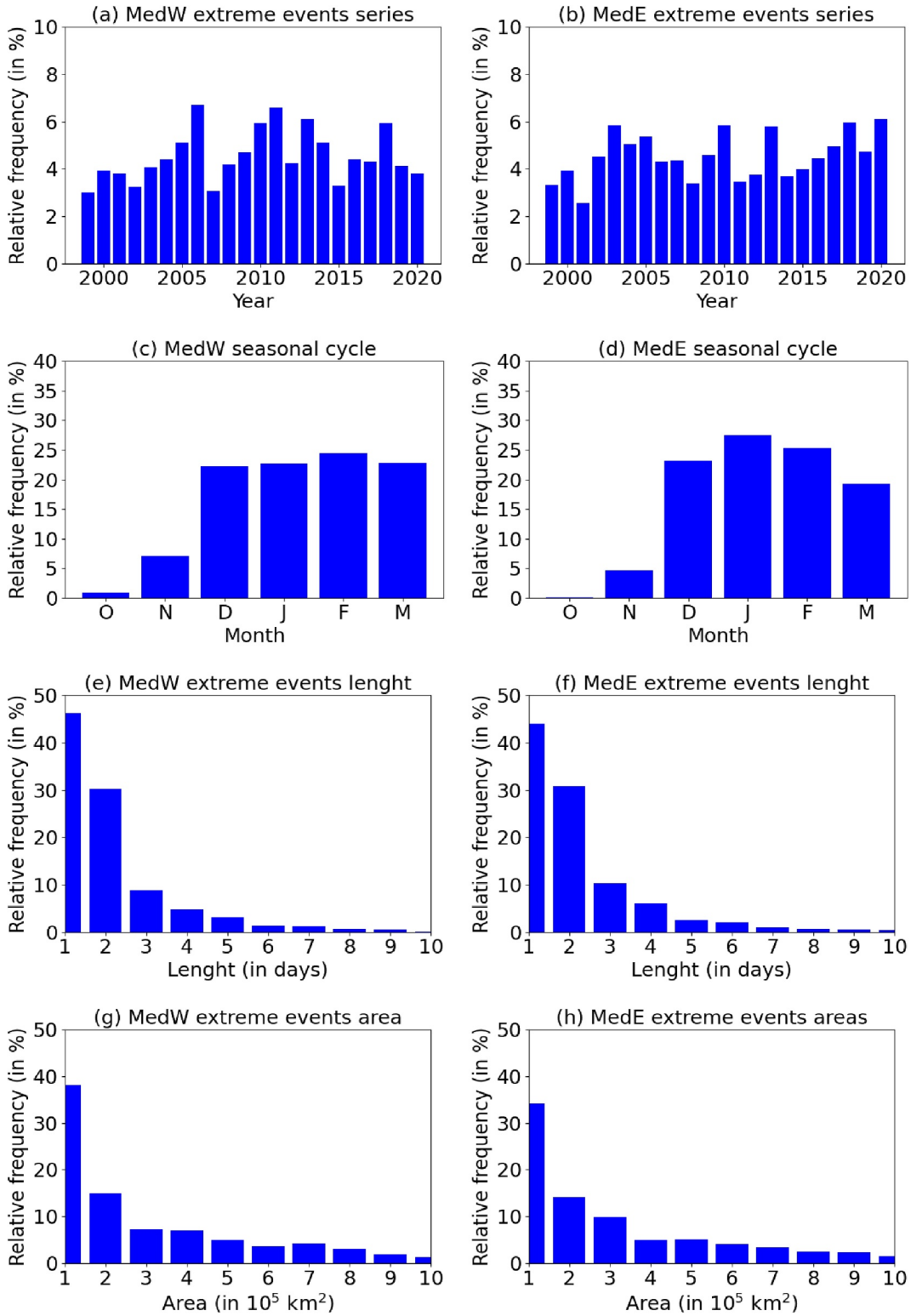

Figure 3. 1999–2020 ONDJFM time series (as relative frequency in %, a, b), seasonal cycle (as relative frequency in %, c, d), and relative frequency (in %) of EEs in function of their length (in days, e,f) and average area (in km^2, g, h) in MedW (a, c, e, g) and MedE (b, d, f, h).

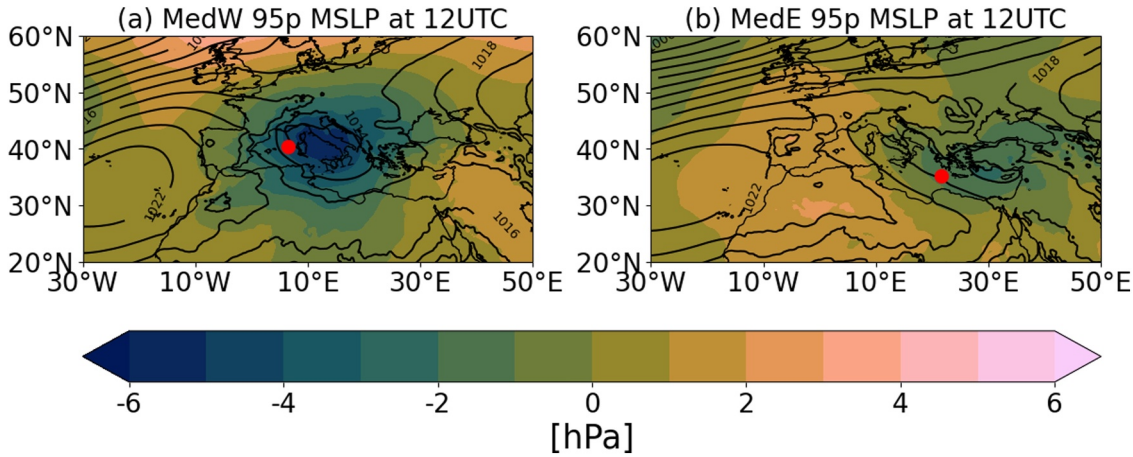

Figure 4. Composite of mean sea level pressure (MSLP) (contour lines, in hPa) at 12 UTC on the day of the centroid in the period 1999–2020 for EEs in MedW (a) and MedE (b). Shaded colors are the anomalies (in hPa) of the composite of MSLP with respect to 1999–2020 ONDJFM climatology.

both MedW and MedE, the large-scale configurations observed in Figure 4 produces, as expected, stronger (colder)-than-average wind speed (2 m temperature). In MedW, the anomalies in the wind speed, whose maximum coincides with the location of the Mistral wind in the gulf of Lions, can be even greater than 4 m/s with respect to the ONDJFM climatology. Assuming an average speed of 10 m/s in the area, the intensity of wind field associated with the EEs in the gulf of Lions is approximately 50% stronger than the climatological value. The same results hold for the 2 m temperature. During EEs, in both MedW and MedE, temperatures are usually more than 2°C colder than the climatology.

The cooling effects of these air masses that flow over the Mediterranean Sea are shown in Figure 7. Here, the composite and the anomalies of SST with respect to the SST ONDJFM climatology for the period 1999–2020 demonstrate that the EEs occurred with SSTs that are 2°C colder with respect to the climatology (Figure 7).

3.2. Cyclones Producing EEs

Figure 8 shows the density of tracks (contours) of cyclones associated with EEs in MedW (a) and MedE (b), respectively. The domain has been divided into cells of 1.5° size and each cyclone system has been counted in each cell only once while it moves along the track. The units used are relative frequency (in %) of cyclone track crossing each cell of the domain in the 6-hourly field. In MedW, it is evident that cyclone tracks originate from several well-known cyclogenetic areas for the MS, namely the North Africa, Gulf of Genoa (where the maximum

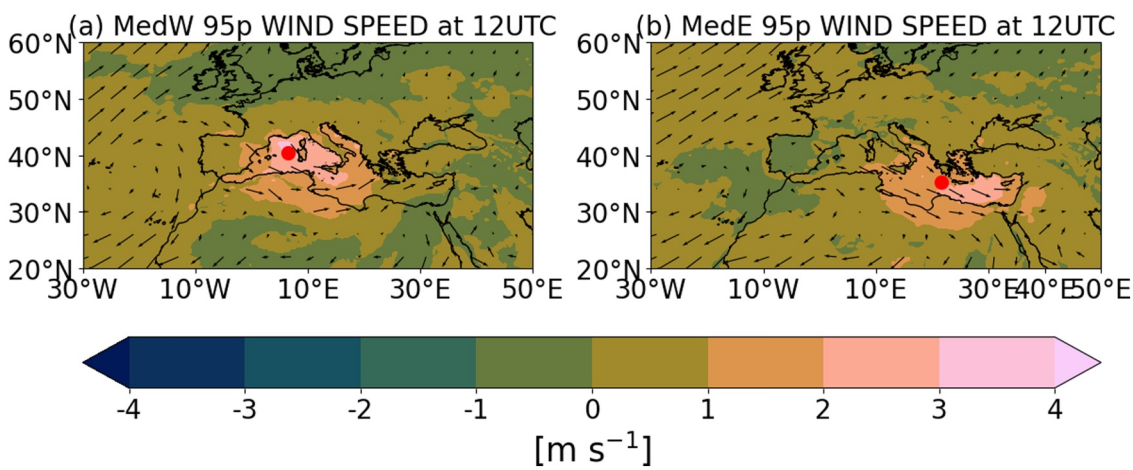

Figure 5. Composite of wind fields (arrows, in m/s) at 12 UTC on the day of the centroid in the period 1999–2020 for EEs in MedW (a) and MedE (b). Shaded colors are the anomalies (m/s) of the composite of wind speed with respect to 1999–2020 ONDJFM climatology.

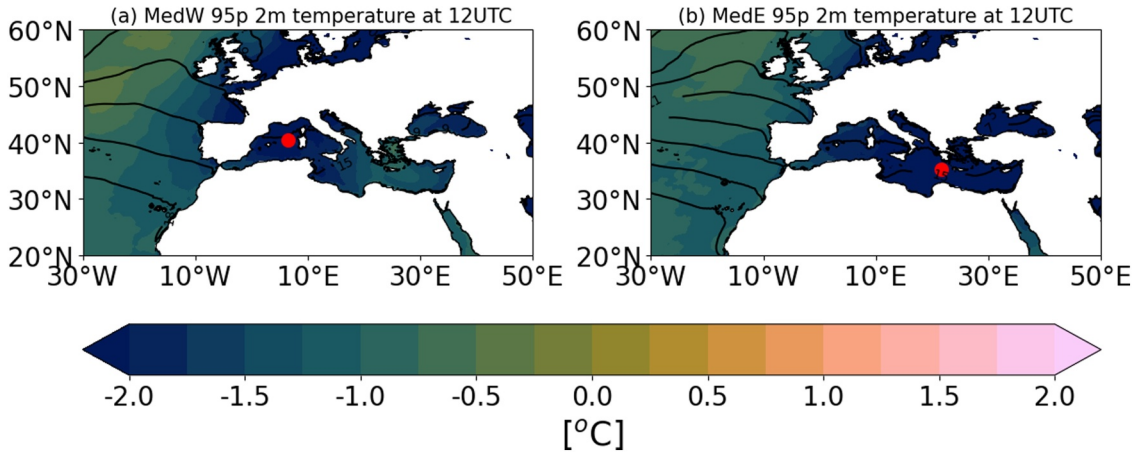

Figure 6. Composite of 2 m temperature (contour lines, in °C) at 12 UTC on the day of the centroid in the period 1999–2020 for EEs in MedW (a) and MedE (b). Shaded colors are the anomalies (in °C) of the composite of 2 m temperature with respect to 1999–2020 ONDJFM climatology. 2 m temperature values over the land have been masked.

of density of tracks is located), and in the northeastern Atlantic (Flaounas et al., 2022, 2023; Lionello et al., 2002, 2016; Lionello et al., 2016, 2019; Nissen et al., 2010, 2014; Reale & Lionello, 2013; Reale et al., 2021; Trigo et al., 1999, 2006). The prevalent motion of the weather systems is north-west/south east along the so-called Mediterranean storm track (Flaounas et al., 2018, 2022, 2023; Lionello et al., 2006, 2016; Ulbrich et al., 2012). In the MedE, the importance of Atlantic cyclones decreases significantly with respect to the MedW while there is the appearance of a maximum in the Levantine Basin that corresponds to the location of the so-called Cyprus lows (e.g., Flaounas et al., 2022; Lionello et al., 2012).

In order to assess the robustness of the strength of the link between cyclones and EEs, we carried out a sensitivity analysis repeating the search of the cyclones but changing the threshold for the detection of high CO_2 sink events (i.e., the percentile threshold). Then, as a reference term for comparison, we apply the same procedure of searching applied to the mean location of the centroid of EE_{70p}, EE_{80p}, EE_{90p}, EE_{95p} in a generic day of the period ONDJFM 1999–2020 (and thus not necessary when a specific EE takes place, hereafter climatological value). In general, the probability of detecting a cyclone within a distance of 15° from the centroid increases with the magnitude of the threshold from 67% in EE_{70p} to 85% in the case of EE_{95p} in MedW and from 70% to 84% in the case of MedE (Table 1, second column). Furthermore, the probability to find a cyclone near the location of the centroid is higher with respect to the climatological value (ProbCLIM, 35%, Table 1, third column). Moreover, considering the cyclogenesis areas defined in Figure 1a, it is clear that most cyclones associated with EE_{70p},

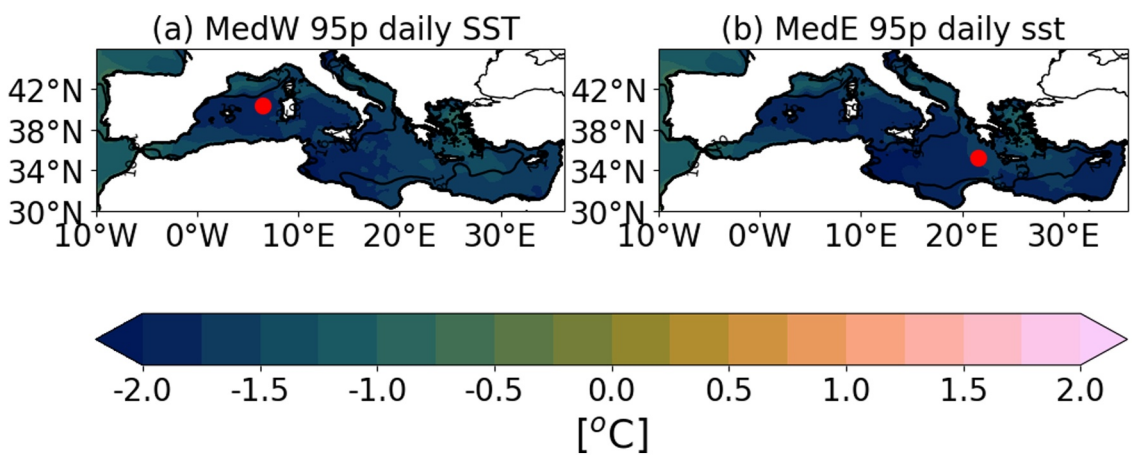

Figure 7. Composite of satellite sea surface temperature (SST) (contour lines, in °C) at 12 UTC on the day of the centroid in the period 1999–2020 for EEs in MedW (a) and MedE(b). Shaded colors are the anomalies (in °C) of the composite of the SST with respect to 1999–2020 ONDJFM climatology.

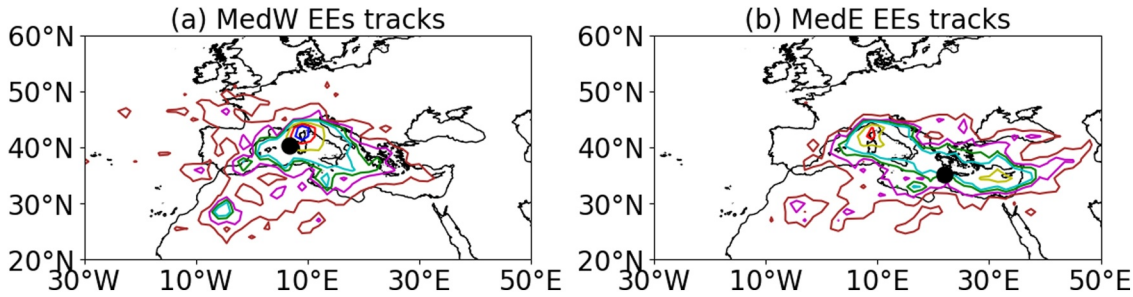

Figure 8. Density of tracks of cyclones associated with EEs in MedW(a) and MedE(b). Black dots represent the mean location of the centroids in each sub-basin. Contour lines are drawn at 0.25 (brown), 0.5 (magenta), 0.75 (green), 1 (cyan), 2 (yellow), 3 (red), and 4 (blue). The units used are relative frequency in % in each cell of 1.5°.

EE_{80p}, EE_{90p}, EE_{95p} originated within MEDIT with a percentage that increases in function of the threshold adopted (Table 1). On the other hand, the percentages tend to decrease for all the other areas, and the contribution of MEDIT (ATLANTICO) is the largest (the smallest) in MedE.

3.3. Characterization of Cyclones Producing EE_{95p}

In order to identify the characteristics of the cyclones associated with EEs, we considered three variables characterizing extratropical cyclones: depth, size, and MSLP gradient. The depth (in hPa) is a measure of the intensity of the cyclone given by the difference between the pressure at the center of the system and the pressure in the background field around the system (see Reale & Lionello, 2013 for more details). The larger the difference, the stronger the system. The size of a cyclone (in km) is defined as follows:

$$\sqrt{\frac{\sum_i d_i^2}{P}} \tag{2}$$

Table 1
Statistics of Cyclones Associated With EE_{70p}, EE_{80p}, EE_{90p}, and EE_{95p} in MedW and MedE

	Cyclones associated with a EEs		Cyclogenesis			
	Prob [%]	ProbCLIM [%]	MEDIT [%]	ATLANTICO [%]	AFRICA [%]	EEMES [%]
MedW						
EE_{70p}	67	35	45(37)	25(26)	23(31)	6(5)
EE_{80p}	72	35	49(37)	27(26)	19(30)	4(6)
EE_{90p}	79	35	50(38)	28(26)	17(28)	3(6)
EE_{95p}	85	35	54(38)	26(26)	15(27)	3(7)
MedE						
EE_{70p}	70	33	61(59)	7(7)	18(21)	12(11)
EE_{80p}	74	33	60(59)	6(7)	22(22)	11(11)
EE_{90p}	80	33	63(59)	7(8)	20(22)	8(9)
EE_{95p}	85	33	66(59)	8(8)	17(23)	7(8)

Note. The columns "Prob" and "ProbCLIM" show the probability (in %) of finding a cyclone within a distance of 15° from the mean location of centroids and the corresponding climatological value. The climatological value is defined as the probability to find a cyclone within a distance of 15° from to the mean location of the centroid of EE_{70p}, EE_{80p}, EE_{90p}, and EE_{95p} in a generic day of the period ONDJFM 1999–2020. The columns MEDIT, ATLANTICO, AFRICA, and EEMES show the probability (%) that the cyclogenesis of the cyclone associated with EE_{70p}, EE_{80p}, EE_{90p}, and EE_{95p} takes place in the areas shown in Figure 1a. The values between brackets are the climatological values.

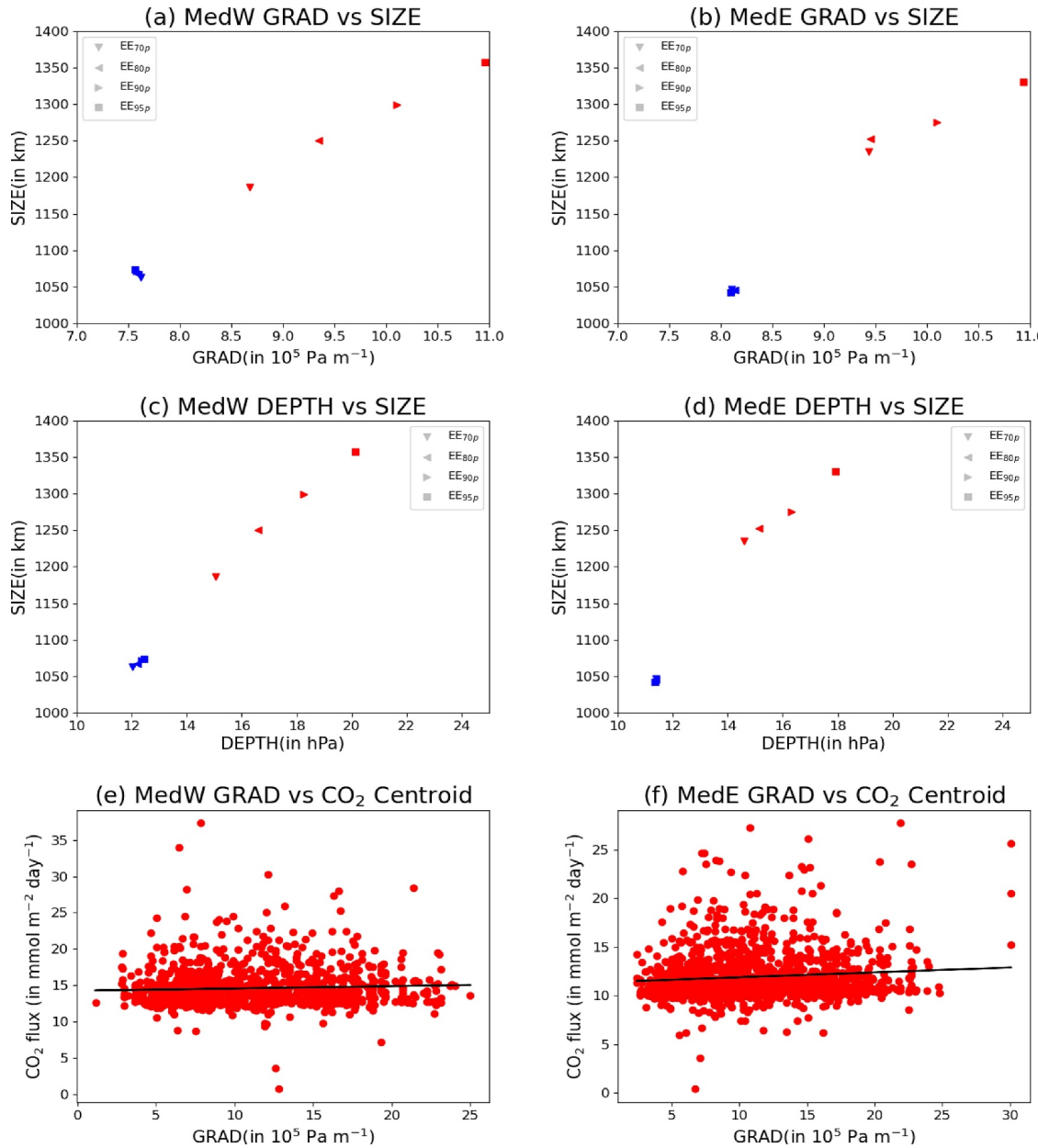

Figure 9. (a, b) Mean Values of Gradient (*x*-axis, in 10^5 Pa m^{-1}) and Size (*y*-axis, in km) of cyclones associated with EE_{70p}, EE_{80p}, EE_{90p}, EE_{95p} (red), and their climatological value (in blue), (c, d) as (a, b) but for Depth (*x*-axis, in hPa) and Size (*y*-axis, in km). The statistical difference between the mean of values for each variable has been tested by using a Mann-Whitney test at 95%. (e, f) Values of Gradient (in 10^5 Pa m^{-1}, *x*-axis) of cyclones and values of CO_2 fluxes in the day of the centroid (in mmol m^{-2} day^{-1}) in EE_{95p} (red dots) and related linear regression (statistically significant with $p < 0.05$, black line).

where d^2_i is the distance of a generic point from the center of the cyclone with P representing the total number of points associated with each cyclone (e.g., Reale et al., 2021; Reale & Lionello, 2013). Finally, the gradient of the cyclone (in hPa m^{-1}) is the maximum value of the MSLP gradient observed within the system.

The mean values of these variables have been computed for all the cyclones associated with EE_{70p}, EE_{80p}, EE_{90p}, EE_{95p}, and then compared with their climatological value, which has been computed for cyclones detected nearby to the mean location of the centroid in a generic day of the period ONDJFM 1999–2020 (as already done in Table 1). The statistical difference between the mean of values for each variable has been tested by using a Mann-Whitney test at 95%. Figures 9a–9d shows the comparison between gradient (depth) and size of the systems associated with EE_{70p}, EE_{80p}, EE_{90p}, EE_{95p}, and their climatological values. In general, both figures show that

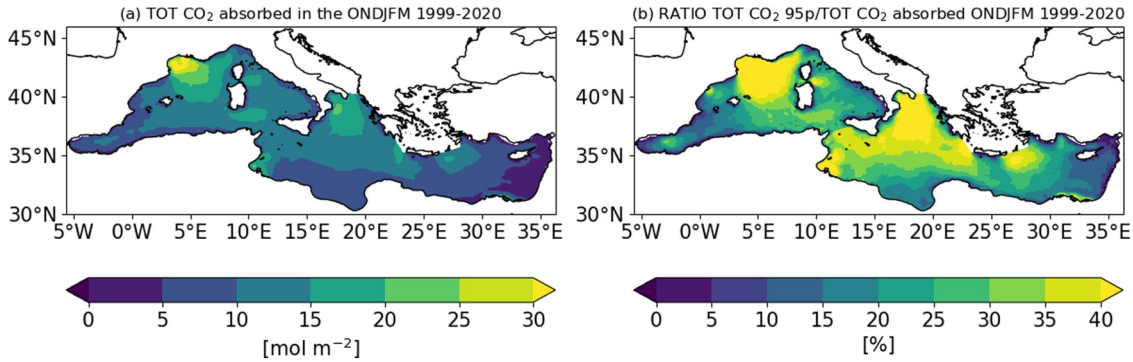

Figure 10. (a) Total CO_2 absorbed in the ONDJFM 1999–2020 (in mol m^{-2}) and (b) ratio (in %) between total CO_2 absorbed in the ONDJFM 1999–2020 and the total CO_2 absorbed during the EEs_{95p} (in %).

these cyclones tend to be bigger, deeper and characterized by a stronger gradient than their climatological counterpart. All these differences are statistically significant.

Figures 9e and 9f confirm the presence of a linear relationship (statistically significant at $p < 0.05$) between the intensity of the atmospheric circulation associated to the cyclone (measured by the maximum MSLP gradient of the system) and the intensity of CO_2 flux at the centroid. In fact, both figures show that the quantity of CO_2 absorbed in the day of the centroid increases with the maximum gradient of the system in both MedW and MedE and thus with the intensity of the circulation (wind) driven by the presence of the cyclone.

Finally, Figures 10a and 10b show the total CO_2 absorbed in the ONDJFM 1999–2020 (a) and the ratio (b) between the CO_2 absorbed during the EE_{95p} and the total CO_2 absorbed in the ONDJFM 1999–2020. It is shown that EE_{95p} accounts for more than 40% of total CO_2 absorbed in the MS in winter between 1999 and 2020. Further, both maps show that the CO_2 sink exhibit some maxima located along the Mediterranean storm track (Flaounas et al., 2022; Lionello et al., 2016) pointing out that a part of capacity of the Mediterranean Sea to absorb atmospheric CO_2 occur in areas marked by a significant synoptic activity.

4. Conclusions

This study analyzed the temporal characteristics of the high CO_2 sink events (EEs) in the MS and investigated a possible association with the passage of extra-tropical cyclones across the MEDIT during the winter season.

The analysis of the large-scale configurations associated with EEs has pointed out the existence of different minima/maxima in the MSLP able to produce stronger (colder) wind (temperature) fields across the MEDIT (Figures 4–7). In fact, as shown in the introduction, CO_2 fluxes are significantly dependent on temperature and wind speed (Equation 1): our analysis has found that these large-scale configurations produce in both western and eastern Mediterranean colder-than-average 2 m air temperature and SST (almost 2°C) and stronger-than-average wind speed (more than 4 m s^{-1} in some areas of the western Mediterranean). Moreover, these configurations suggested the possibility of a link between EEs and the passage of extra-tropical cyclones in the MEDIT. From this point of view, the analysis of the probability of detecting a cyclone within a fixed distance from the mean location of the centroid of the EEs using different thresholds to detect the EE has shown that, in both sub-basins, this probability increases with the magnitude of the EE and is always higher than the climatological values. In most of the cases, these cyclones originated within the MEDIT with a lower contribution from other climatological cyclogenesis areas such the North Atlantic and Northern Africa (e.g., Lionello et al., 2016).

The analysis of the characteristics of the cyclones associated with EEs showed that these systems are usually deeper, bigger and characterized by a stronger circulation with respect to their climatological counterpart. Moreover, the intensity and size of the cyclones associated with the largest events of the CO_2 sink (EE_{95p}) are greater than those of cyclones associated with the lowest intensity in our sensitivity analysis (EE_{70p}). The magnitude of CO_2 sink increases with the intensity of the system, which is somehow something to be expected due to the strong links between CO_2 air-sea fluxes and wind field and between wind field intensity and extra-tropical cyclones intensity (measured by the maximum of MSLP gradient).

Finally, the analysis pointed out that EE_{95p} account, in many areas of the basin, for more than 40% of the total CO_2 absorbed in winter in the Mediterranean Sea suggesting that, in the view of the links between cyclones and high CO_2 sink events, an assessment of the carbon budget of the basin needs to account for the synoptic activity in the region.

Climate projections based on ensemble of CMIP5 GCMs and regional coupled system models under business-as-usual emission scenario (RCP8.5) have showed a decrease between 25% and 50% of the frequency of extratropical cyclones crossing the MEDIT and a decrease in their intensity and size (Reale et al., 2021; Zappa et al., 2015). By projecting the link highlighted in our analysis between the magnitude of CO_2 sink and cyclones characteristics to future change in cyclone activity in the MEDIT, it could be expected for the next decades a significant reduction in the capabilities of MS to act as a sink for the anthropogenic carbon. This potential signal, combined with the basin warming under a high atmospheric CO_2 scenario (Reale et al., 2022; Soto-Navarro et al., 2020), could reduce the capacity of MS to contribute to CO_2 sequestration.

The assessment of possible changes under different emission scenarios of the link between CO_2 air-sea fluxes and cyclone activity in the MEDIT will require the adoption of proper modeling tools such as Earth System models. Moreover, a more complete analysis will need to include also the outgassing events that in the present work have not been considered.

Conflict of Interest

The authors declare no conflicts of interest relevant to this study.

Data Availability Statement

All data used are open and publicly available: ERA5 data are available from Copernicus Climate Change Service (C3S) Climate Data Store (CDS) (Hersbach et al., 2023). The daily high resolution L4 SST reprocessed long-term SST and the CMS biogeochemical reanalysis data set are available from the Copernicus Marine Service (Cossarini et al., 2021; Embury et al., 2024; Pisano et al., 2016).

Acknowledgments

This work has been supported by OGS and CINECA under the High-Performance Computing Training and Research for Earth Sciences (HPC-TRES) program founded by PRACE-Italy National Research Infrastructure. This study has been conducted using E.U. Copernicus Marine Service Information https://doi.org/10.48670/moi-00173 and https://doi.org/10.48670/mds-00374. M. Reale was supported by the National Recovery and Resilience Plan project TeRABIT (Terabit network for Research and Academic Big data in Italy–IR0000022–PNRR Missione 4, Componente 2, Investimento 3.1 CUP I53C21000370006) in the frame of the European Union–NextGenerationEU funding. F.Giordano was supported by the project iNEST – Interconnected Nord-Est Innovation Ecosystem, funded by the European Union – NextGenerationEU (ECS00000043 – CUP J43C22000320006). We acknowledge the CINECA award under the ISCRA initiative and the supercomputing resources and support from ICSC—Centro Nazionale di Ricerca in High Performance Computing, Big Data and Quantum Computing—Spoke 4 Earth and Climate and hosting entity, funded by European Union—NextGenerationEU. This work is a contribution to the COST Action CA19109 "MedCyclones: European Network for Mediterranean Cyclones in weather and climate".

References

Álvarez, M., Catalá, T. S., Civitarese, G., Coppola, L., Hassoun, A. E., Ibello, V., & Ulses, C. (2023). Mediterranean Sea general biogeochemistry. In *Oceanography of the Mediterranean Sea* (pp. 387–451). Elsevier.

Álvarez, M., Sanleón-Bartolomé, H., Tanhua, T., Mintrop, L., Luchetta, A., Cantoni, C., et al. (2014). The CO_2 system in the Mediterranean Sea: A basin wide perspective. *Ocean Science*, *10*(1), 69–92. https://doi.org/10.5194/os-10-69-2014

Buzzi, A., Davolio, S., & Fantini, M. (2020). Cyclogenesis in the lee of the alps: A review of theories. *Bulletin of Atmospheric Science and Technology*, *1*(3–4), 433–457. https://doi.org/10.1007/s42865-020-00021-6

Campins, J., Genoveìs, A., Picornell, M. A., & Jansà, A. (2011). Climatology of Mediterranean cyclones using the ERA-40 dataset. *International Journal of Climatology*, *31*, 1596–1614. https://doi.org/10.1002/joc.2183

Canu, D. M., Ghermandi, A., Nunes, P. A., Lazzari, P., Cossarini, G., & Solidoro, C. (2015). Estimating the value of carbon sequestration ecosystem services in the Mediterranean Sea: An ecological economics approach. *Global Environmental Change*, *32*, 87–95. https://doi.org/10.1016/j.gloenvcha.2015.02.008

Carracedo, L. I., Pérez, F. F., Gilcoto, M., Velo, A., Padín, A., & Rosón, G. (2018). Role of the circulation on the anthropogenic CO2 inventory in the north-east Atlantic: A climatological analysis. *Progress in Oceanography*, *161*, 78–86. https://doi.org/10.1016/j.pocean.2018.01.009

Carranza, M. M., Long, M. C., Di Luca, A., Fassbender, A. J., Johnson, K. S., Takeshita, Y., et al. (2024). Extratropical storms induce carbon outgassing over the Southern Ocean. *npj Climate and Atmospheric Science*, *7*(1), 106. https://doi.org/10.1038/s41612-024-00657-7

Clementi, E. (2022). The September 2020 medicane ianos predicted by the mediterranean forecasting systems. *Copernicus ocean state report, 6. J. Oper. Oceanogr*, *15*(1), s185–s192.

Cossarini, G., Feudale, L., Teruzzi, A., Bolzon, G., Coidessa, G., Solidoro, C., et al. (2021). High-resolution Reanalysis of the Mediterranean Sea biogeochemistry (1999–2019). *Frontiers in Marine Science*, *8*, 741486. https://doi.org/10.3389/fmars.2021.741486

Cossarini, G., Lazzari, P., & Solidoro, C. (2015). Spatiotemporal variability of alkalinity in the Mediterranean Sea. *Biogeosciences*, *12*(6), 1647–1658. https://doi.org/10.5194/bg-12-1647-2015

Crise, A., Allen, J., Baretta, J., Crispi, G., Mosetti, R., & Solidoro, C. (1999). The Mediterranean pelagic ecosystem response to physical forcing. *Progress in Oceanography*, *44*(1–3), 219–243. https://doi.org/10.1016/s0079-6611(99)00027-0

Crispi, G., Mosetti, R., Solidoro, C., & Crise, A. (2001). Nutrient cycling in Mediterranean basins: The role of the biological pump in the trophic regime. *Ecological Modelling*, *138*(1–3), 101–114. https://doi.org/10.1016/s0304-3800(00)00396-3

De la Vara, A., Gutiérrez-Fernández, J., González-Alemán, J. J., & Gaertner, M. Á. (2021). Characterization of medicanes with a minimal number of geopotential levels. *International Journal of Climatology*, *41*, 3300–3316. https://doi.org/10.1002/joc.7020

Di Biagio, V. (2017). *A method to characterize the statistical extremes in marine biogeochemistry: The case of the mediterranean chlorophyll, PhD thesis*. Università degli Studi di Trieste. Retrieved from http://hdl.handle.net/11368/2908150

Di Biagio, V., Cossarini, G., Salon, S., & Solidoro, C. (2020). Extreme event waves in marine ecosystems: An application to Mediterranean Sea surface chlorophyll. *Biogeosciences*, *17*(23), 5967–5988. https://doi.org/10.5194/bg-17-5967-2020

Doensen, O., Messmer, M., Kim, W. M., & Raible, C. C. (2025). Characterization of the mean and extreme Mediterranean cyclones and their variability during the period 1500 BCE to 1850 CE. *Climate of the Past*, *21*(7), 1305–1322. https://doi.org/10.5194/cp-21-1305-2025

D'Ortenzio, F., Antoine, D., & Marullo, S. (2008). Satellite-driven modeling of the upper ocean mixed layer and air–sea CO_2 flux in the Mediterranean Sea. *Deep Sea Research Part I: Oceanographic Research Papers*, *55*(4), 405–434. https://doi.org/10.1016/j.dsr.2007.12.008

Emanuel, K., Alberti, T., Bourdin, S., Camargo, S. J., Faranda, D., Flaounas, E., et al. (2025). CYCLOPs: A unified framework for surface flux-driven cyclones outside the tropics. *Weather and Climate Dynamics*, *6*(3), 901–926. https://doi.org/10.5194/wcd-6-901-2025

Embury, O., Merchant, C. J., Good, S. A., Rayner, N. A., Høyer, J. L., Atkinson, C., et al. (2024). Satellite-based time-series of sea-surface temperature since 1980 for climate applications. *Scientific Data*, *11*(1), 326. https://doi.org/10.1038/s41597-024-03147-w

Escudier, R., Clementi, E., Cipollone, A., Pistoia, J., Drudi, M., Grandi, A., et al. (2021). A high resolution reanalysis for the Mediterranean Sea. *Frontiers of Earth Science*, *9*, 702285. https://doi.org/10.3389/feart.2021.702285

Flaounas, E., Aragão, L., Bernini, L., Dafis, S., Doiteau, B., Flocas, H., et al. (2023). A composite approach to produce reference datasets for extratropical cyclone tracks: Application to Mediterranean cyclones. *Weather and Climate Dynamics*, *4*(3), 639–661. https://doi.org/10.5194/wcd-4-639-2023

Flaounas, E., Davolio, S., Raveh-Rubin, S., Pantillon, F., Miglietta, M. M., Gaertner, M. A., et al. (2022). Mediterranean cyclones: Current knowledge and open questions on dynamics, prediction, climatology and impacts. *Weather Clim. Dynam.*, *3*(1), 173–208. https://doi.org/10.5194/wcd-3-173-2022

Flaounas, E., Kelemen, F. D., Wernli, H., Gaertner, M. A., Reale, M., Sanchez-Gomez, E., et al. (2018). Assessment of an ensemble of ocean–atmosphere coupled and uncoupled regional climate models to reproduce the climatology of mediterranean cyclones. *Climate Dynamics*, *51*(3), 1023–1040. https://doi.org/10.1007/s00382-016-3398-7

Frangoulis, C., Stamataki, N., Pettas, M., Michelinakis, S., King, A. L., Giannoudi, L., et al. (2024). A carbonate system time series in the eastern Mediterranean Sea. Two years of high-frequency in-situ observations and remote sensing. *Frontiers in Marine Science*, *11*, 1348161. https://doi.org/10.3389/fmars.2024.1348161

Giordano, F., Querin, S., Reini, M., & Salon, S. (2024). High-resolution modelling of a shallow marginal sea to assess the potential of energy production from marine currents: The northern adriatic sea case study. *Bulletin of the Geophysical Observatory*. https://doi.org/10.4430/bgo00466

Gutiérrez-Loza, L., Nilsson, E., Wallin, M. B., Sahlée, E., & Rutgersson, A. (2022). On physical mechanisms enhancing air–sea CO_2 exchange. *Biogeosciences*, *19*(24), 5645–5665. https://doi.org/10.5194/bg-19-5645-2022

Hersbach, H., Bell, B., Berrisford, P., Biavati, G., Horányi, A., Muñoz Sabater, J., et al. (2023). ERA5 hourly data on single levels from 1940 to present. *Copernicus Climate Change Service (C3S) Climate Data Store (CDS)*. https://doi.org/10.24381/cds.adbb2d47

Hersbach, H., Bell, B., Berrisford, P., Hirahara, S., Horányi, A., Muñoz-Sabater, J., et al. (2020). The ERA5 global reanalysis. *Quarterly Journal of the Royal Meteorological Society*, *146*(730), 1999–2049. https://doi.org/10.1002/qj.3803

Jangir, B., Mishra, A. K., & Strobach, E. (2024). The interplay between medicanes and the Mediterranean Sea in the presence of sea surface temperature anomalies. *Atmospheric Research*, *310*, 107625. https://doi.org/10.1016/j.atmosres.2024.107625

Kendall, M. G. (1975). In *Rank correlation methods* (4th ed.). Charles Griffin.

Lazzari, P., Solidoro, C., Ibello, V., Salon, S., Teruzzi, A., Béranger, K., et al. (2012). Seasonal and inter-annual variability of plankton chlorophyll and primary production in the Mediterranean Sea: A modelling approach. *Biogeosciences*, *9*(1), 217–233. https://doi.org/10.5194/bg-9-217-2012

Lazzari, P., Solidoro, C., Salon, S., & Bolzon, G. (2016). Spatial variability of phosphate and nitrate in the Mediterranean Sea: A modeling approach. *Deep-Sea Research*, *108*, 39–52. https://doi.org/10.1016/j.dsr.2015.12.006

Lionello, P., Abrantes, F., Congedi, L., Dulac, F., Gaci′c, M., Gomis, D., et al. (2012). Introduction: Mediterranean climate: Background information. In P. Lionello (Ed.), *The climate of the mediterranean region. From the past to the future*. Elsevier.

Lionello, P., Bhend, J., Buzzi, A., Della-Marta, P. M., Krichak, S. O., Jansà, A., et al. (2006). Chapter 6: Cyclones in the Mediterranean region: Climatology and effects on the environment. In *Developments in Earth and environmental sciences* (Vol. 4, pp. 325–372). Elsevier. Available from. https://doi.org/10.1016/S1571-9197(06)80009-1

Lionello, P., Conte, D., & Reale, M. (2019). The effect of cyclones crossing the mediterranean region on sea level anomalies on the Mediterranean Sea Coast. *Natural Hazards and Earth System Sciences*, *19*(7), 1541–1564. https://doi.org/10.5194/nhess-19-1541-2019

Lionello, P., Dalan, F., & Elvini, E. (2002). Cyclones in the Mediterranean region: The present and the doubled CO_2 climate scenarios. *Climate Research*, *22*, 147–159. https://doi.org/10.3354/cr022147

Lionello, P., Trigo, I. F., Gil, V., Liberato, M. L. R., Nissen, K. M., Pinto, J. G., et al. (2016). Objective climatology of cyclones in the Mediterranean region: A consensus view among methods with different system identification and tracking criteria. *Tellus A: Dynamic Meteorology and Oceanography*, *68*(1), 29391. Available from. https://doi.org/10.3402/tellusa.v68.29391

Mann, H. B. (1945). Non-parametric tests against trend. *Econometrica*, *13*(3), 163–171. https://doi.org/10.2307/1907187

Martinez, A., & Iglesias, G. (2023). Climate-change impacts on offshore wind resources in the Mediterranean Sea. *Energy Conversion and Management*, *291*, 117231. https://doi.org/10.1016/j.enconman.2023.117231

Menna, M., Martellucci, R., Reale, M., Cossarini, G., Salon, S., Notarstefano, G., et al. (2023). A case study of impacts of an extreme weather system on the Mediterranean Sea circulation features: Medicane Apollo (2021). *Scientific Reports*, *13*(1), 3870. https://doi.org/10.1038/s41598-023-29942-w

Nissen, K. M., Leckebusch, G. C., Pinto, J. C., Renggli, D., Ulbrich, S., & Ulbrich, U. (2010). Cyclones causing wind storms in the Mediterranean: Characteristics, trends and links to large-scale patterns. *Natural Hazards and Earth System Sciences*, *10*(7), 1379–1391. https://doi.org/10.5194/nhess-10-1379-2010

Nissen, K. M., Leckebusch, G. C., Pinto, J. C., & Ulbrich, U. (2014). Mediterranean cyclones and windstorms in a changing climate. *Regional Environmental Change*, *14*(5), 1873–1890. https://doi.org/10.1007/s10113-012-0400-8

Pisano, A., Nardelli, B. B., Tronconi, C., & Santoleri, R. (2016). The new mediterranean optimally interpolated pathfinder AVHRR SST dataset (1982–2012). *Remote Sensing of Environment*, *176*, 107–116. https://doi.org/10.1016/j.rse.2016.01.019

Portal, A., Raveh-Rubin, S., Catto, J. L., Givon, Y., & Martius, O. (2024). Linking compound weather extremes to Mediterranean cyclones, fronts, and airstreams. *Weather and Climate Dynamics*, *5*(3), 1043–1060. https://doi.org/10.5194/wcd-5-1043-2024

Ragone, F., Meli, A., Napoli, A., & Pasquero, C. (2019). Ocean surface anomalies after strong winds in the Western Mediterranean Sea. *Journal of Marine Science and Engineering*, *7*(6), 182. https://doi.org/10.3390/jmse7060182

Raveh-Rubin, S., & Wernli, H. (2015). Large-scale wind and precipitation extremes in the Mediterranean: A climatological analysis for 1979–2012. *Quarterly Journal of the Royal Meteorological Society*, *141*(691), 2404–2417. https://doi.org/10.1002/qj.2531

Reale, M., Cabos Narvaez, W. D., Cavicchia, L., Conte, D., Coppola, E., Flaounas, E., et al. (2021). Future projections of Mediterranean cyclone characteristics using the Med-CORDEX ensemble of coupled regional climate system models. *Climate Dynamics*, *58*(9–10), 1–24. https://doi.org/10.1007/s00382-021-06018-x

Reale, M., Cossarini, G., Lazzari, P., Lovato, T., Bolzon, G., Masina, S., et al. (2022). Acidification, deoxygenation, and nutrient and biomass declines in a warming Mediterranean Sea, *Biogeosciences*, *19*, 4035–4065. https://doi.org/10.5194/bg-19-4035-2022

Reale, M., Giorgi, F., Solidoro, C., Di Biagio, V., Di Sante, F., Mariotti, L., et al. (2020). The regional Earth system model RegCM-ES: Evaluation of the Mediterranean climate and marine biogeochemistry. *Journal of Advances in Modeling Earth Systems*, *12*(9), e2019MS001812. https://doi.org/10.1029/2019ms001812

Reale, M., & Lionello, P. (2013). Synoptic climatology of winter intense precipitation events along the Mediterranean coasts. *Natural Hazards and Earth System Sciences*, *13*(7), 1707–1722. https://doi.org/10.5194/nhess-13-1707-2013

Reale, M., Salon, S., Somot, S., Solidoro, C., Giorgi, F., Crise, A., et al. (2020). Influence of large-scale atmospheric circulation patterns on nutrient dynamics in the Mediterranean Sea in the extended winter season (October-March) 1961-1999. *Climate Research*, *82*, 117–136. https://doi.org/10.3354/cr01620

Salon, S., Cossarini, G., Bolzon, G., Feudale, L., Lazzari, P., Teruzzi, A., et al. (2019). Novel metrics based on biogeochemical argo data to improve the model uncertainty evaluation of the CMEMS Mediterranean marine ecosystem forecasts. *Ocean Science*, *15*(4), 997–1022. https://doi.org/10.5194/os-15-997-2019

Schroeder, K., Garcìa-Lafuente, J., Josey, S. A., Artale, V., Nardelli, B. B., Carrillo, A., et al. (2012). Circulation of the Mediterranean Sea and its variability. In P. Lionello (Ed.), *The climate of the mediterranean region: From the past to the future* (pp. 187–256). Elsevier Inc. https://doi.org/10.1016/B978-0-12-416042-2.00003-3

Siokou-Frangou, I., Christaki, U., Mazzocchi, M. G., Montresor, M., Ribera d'Alcalá, M., Vaqué, D., & Zingone, A. (2010). Plankton in the open Mediterranean Sea: A review. *Biogeosciences*, *7*(5), 1543–1586. https://doi.org/10.5194/bg-7-1543-2010

Soto-Navarro, J., Jordá, G., Amores, A., Cabos, W., Somot, S., Sevault, F., et al. (2020). Evolution of Mediterranean Sea water properties under climate change scenarios in the Med-CORDEX ensemble. *Climate Dynamics*, *54*(3–4), 2135–2165. https://doi.org/10.1007/s00382-019-05105-4

Stambler, N. (2014). The Mediterranean Sea – Primary productivity. In S. Goffredo & Z. Dubinsky (Eds.), *The Mediterranean Sea*. Springer. https://doi.org/10.1007/978-94-007-6704-1_7

Teruzzi, A., Bolzon, G., Salon, S., Lazzari, P., Solidoro, C., & Cossarini, G. (2019). Assimilation of coastal and open sea biogeochemical data to improve phytoplankton simulation in the Mediterranean Sea. *Ocean Model*, *132*(2018), 46–60. https://doi.org/10.1016/j.ocemod.2018.09.007

Teruzzi, A., Di Biagio, V., Feudale, L., Bolzon, G., Lazzari, P., Salon, S., et al. (2021). Mediterranean Sea biogeochemical reanalysis (CMEMS MED-Biogeochemistry, MedBFM3 system) (version 1) [Dataset]. *Copernicus Monitoring Environment Marine Service (CMEMS)*. https://doi.org/10.25423/CMCC/MEDSEA_MULTIYEAR_BGC_006_008_MEDBFM3

Teruzzi, A., Feudale, L., Bolzon, G., Lazzari, P., Salon, S., Di Biagio, V., et al. (2021). Mediterranean Sea biogeochemical reanalysis (CMEMS MED-Biogeochemistry, MedBFM3 system) (version 1) copernicus monitoring environment Marine Service (CMEMS) [dataset]. https://doi.org/10.25423/CMCC/MEDSEA_MULTIYEAR_BGC_006_008_MEDBFM3I

Trigo, I. F. (2006). Climatology and interannual variability of storm tracks in the euro-atlantic sector: A comparison between ERA-40 and NCEP/NCAR reanalyses. *Clim. Clim. Dyn.*, *26*(2–3), 127–143. https://doi.org/10.1007/s00382-005-0065-9

Trigo, I. F., Davies, T. D., & Bigg, G. R. (1999). Objective climatology of cyclones in the mediterranean region. *Journal of Climate*, *12*(6), 1685–1696. https://doi.org/10.1175/1520-0442(1999)012<1685:ococit>2.0.co;2

Ulbrich, U., Lionello, P., Belušic′D, J. J., Knippertz, P., Kuglitsch, F., Leckebusch, G. C., et al. (2012). Climate of the mediterranean: Synoptic patterns, temperature, precipitation, winds, and their extremes. In P. Lionello (Ed.), *The climate of the mediterranean region. From the past to the future* (pp. 301–346). Elsevier.

Vichi, M., Lovato, T., Butenschön, M., Tedesco, L., Lazzari, P., Lazzari, P., et al. (2020). The biogeochemical Flux Model (BFM): Equation description and user manual in BFM version 5.2 BFM report series N. 1. Release 1.2, BFM report series N. 1. Bologna (Vol. *87*). Available online at: http://bfm-community.eu

Wanninkhof, R. (2014). Relationship between wind speed and gas exchange over the ocean revisited. *Limnology and Oceanography: Methods*, *12*(6), 351–362. https://doi.org/10.4319/lom.2014.12.351

Weiss, R. (1974). Carbon dioxide in water and seawater: The solubility of a non-ideal gas. *Marine Chemistry*, *2*(3), 203–215. https://doi.org/10.1016/0304-4203(74)90015-2

Zappa, G., Hawcroft, M. K., Shaffrey, L., Black, E., & Brayshaw, D. J. (2015). Extratropical cyclones and the projected decline of winter mediterranean precipitation in the CMIP5 models. *Climate Dynamics*, *45*(7–8), 1727–1738. https://doi.org/10.1007/s00382-014-2426-8